INTERNATIONAL JOURNAL FOR NUMERICAL METHODS IN FLUIDS, VOL. 6, 479–493 (1986)

MESH EFFECTS ON THE COMPUTATION OF NON-LINEAR GRAVITY WAVES OF ARBITRARY DISCHARGE

E. F. TORO*

College of Aeronautics, Cranfield Institute of Technology, Cranfield, Beds. MK43 0AL, U.K.

SUMMARY

Numerical computations of non-linear gravity waves are presented and the effects of mesh variations on the results are discussed.

Waves are regarded as two-parameter families $(\lambda, A)_Q$ of arbitrary discharge Q, and computations are carried out using a new Kantorovich algorithm.

Mesh effects are to a large extent dependent on the particular wave region under consideration. Three such regions are identified and typical examples are computed and discussed.

KEY WORDS Gravity Waves Kantorovich Method Mesh Effects

1. INTRODUCTION

Theoretical modelling of free-surface gravity waves has made remarkable advances in recent times[1–6] particularly during the last decade. Such progress is due to the development and application of numerical techniques, and the availability of the computing power to solve the governing non-linear equations to high accuracy. A number of surprising results have been obtained which have disproved some suppositions held true for a long time. For instance, it had been assumed that integral quantities such as speed, energy and momentum would increase monotonically with wave height until the highest wave is reached, that periodic solutions would be unique, etc.

Here we are concerned with the steady free-surface gravity wave problem in two dimensions with the physical effects of compressibility, viscosity, rotation and surface tension excluded. This problem, although more simple, retains the full non-linearity of the free-surface boundary condition and constitutes a challenge to the convergence, stability and accuracy of numerical methods. More general gravity-wave problems may be dealt with only after satisfactory treatment of this simple case. Today, it would appear as if such wave problems, particularly from the point of view of the high accuracy achieved (order 110, see for instance Reference 3) and the new wave properties discovered, have been completely solved. From the point of view of the numerical techniques however, with regard to their reliability, simplicity and applicability to more general problems of engineering as well as their scientific interest, there is still scope for further development.

Traditionally, perturbation expansion techniques, as for example those first used by Stokes, have for a long time dominated the field. Modern versions, such as those developed recently by

* Formerly at the University of Leeds, Department of Applied Mathematical Studies, Leeds LS2 9JT, U.K.

0271–2091/86/060479–15$07.50

Received February 1985
Revised February 1986

Schwartz,[2] Cokelet[3] and others, have made use of Pade approximates and adequately chosen expansion parameters to sum up the series. Reported results of applications of these methods to waves on a horizontal bed are indeed very impressive, particularly on account of the accuracy achieved. It is stated, however, that convergence is difficult for large-amplitude waves in the cnoidal and shallow water regions.[2,3] In fact, divergence occurs for a range of waves. Williams[6] has recently used an improved integral equation technique to compute the waves of greatest height for the full range of wavelengths, with the exception of the highest solitary wave which is obtained by extrapolation.

Finite element methods, after their successful performance in structural problems, have gone a long way into the area of fluid mechanics. Their great flexibility, relative simplicity and sound theoretical basis make finite elements a robust and promising method for fluid problems. The utility of these methods is further enhanced by the combined use of variational methods. Since the wave problem under consideration in this paper can be formulated variationally,[7] finite element methods can be applied successfully[8-11] to gravity waves on a horizontal bed, but more importantly to other free-surface gravity flows on more general bed configurations such as steps, weirs, spillways, etc.

In this paper we apply to the wave problem a technique[12] that belongs to the family of finite element methods. This technique is based on a variational principle[7] valid for waves of all amplitudes and wavelengths. The principal objective of the present study is, through numerical experiments, to observe the effects that meshes may have on the computation of gravity waves. The assessment of mesh effects is made by focusing our attention on the wave amplitude A for prescribed values of the wavelength λ and discharge Q. One can interpret the wave problem as a two-parameter bifurcation problem[13] with bifurcation branches $(\lambda, A)_Q$ emanating from the trivial solution at a bifurcation point $\lambda = \lambda_0$ that can be found from the Stokesian linear theory.

Mesh effects on the computation of the curves $(\lambda, A)_Q$ for a range of values of the parameters Q and λ, particularly for the large amplitude section of the curves, will be the main theme of this paper. The effect of mesh variations on other wave properties such as velocity, steepness, etc., will only be considered tangentially. The mesh variations considered are mesh size (mesh refinement) and mesh aspect ratio. Assessment of discretization errors is carried out by observing the total head error (using the dynamic boundary condition) and by comparing results with those of Cokelet[3] and the cnoidal wave theory of Benjamin and Lighthill.[14]

It is found that mesh refinements are, to a large extent, dependent on the behaviour of the branches $(\lambda, A)_Q$, i.e. the bifurcation pattern. Three wave regions (whose precise limits are given in Reference 13) B_1, B_2 and B_3 exist (Figure 8). In B_1 bifurcation is to the left, i.e. the wave amplitude A increases as wavelength decreases, for a fixed value of the discharge Q. B_1 constitutes a deep-water region. In B_3 bifurcation is to the right, i.e. A increases monotonically with λ, for fixed Q. This is a shallow-water wave region. In B_2 bifurcation is to the right and there are turning points at large amplitudes.

In regions B_1 and B_3 relatively coarse meshes may provide an accurate representation of the curves $(\lambda, A)_Q$, provided adequate mesh aspect ratios are observed. In B_2, however, only fine meshes can give reliable results for the curves. For waves of small to moderate amplitude, the lower part of the curves, coarse meshes prove to be generally satisfactory.

For wave properties such as steepness and velocity, fine meshes must be used in all three regions B_1, B_2 and B_3, particularly if double values of solutions are to be detected near to the breaking point.

The aspect ratio R is another important mesh parameter in respect of which the wave regions B_1, B_2 and B_3 have quite distinct requirements. The correct value of R should be chosen before performing mesh refinements. Inadequate R values can give a poor representation of the curves

$(\lambda, A)_Q$ even for the case of limiting small amplitude waves.[15] Generally, fine resolution in the y-direction is required in B_1, whereas in B_3 this resolution requirement is on the x-direction.

2. STATEMENT OF THE PROBLEM

In this paper we are concerned with the effect of meshes on the numerical computation of large-amplitude surface gravity waves on a horizontal bed. Flows are assumed to be two-dimensional, steady, incompressible and irrotational. We also assume that effects of viscosity and surface tension can be neglected.

It can be shown[7] that solutions of the wave problem as stated here are stationary points of the functional

$$J_{Q,\lambda}(h(x), \psi(x, y)) = \int_0^{\lambda} \int_{b(x)}^{b(x)+h(x)} (\tfrac{1}{2}(\nabla\psi)^2 - y)\, dx\, dy, \tag{1}$$

with constraints

$$\begin{aligned} &\psi = Q \text{ on } y = b(x)\text{: the bed,} \\ &\psi = 0 \text{ on } y = b(x) + h(x)\text{: the free surface.} \end{aligned} \tag{2}$$

All quantities in (1) and (2) have been non-dimensionalized with respect to length H_0, the total head or stagnation level, and time $(H_0/g)^{1/2}$, where g denotes the acceleration due to gravity.

In equation (1) Q denotes the discharge and λ denotes the length of the flow domain. Both Q and λ are parameters of the problem whose values are prescribed. The arguments $h(x)$ and $\psi(x\,y)$ of J denote the position of the free surface and the stream function, respectively. $\psi(x, y)$ governs the internal flow field distribution. Both $h(x)$ and $\psi(x, y)$ are to be computed.

Boundary conditions at the inlet and outlet boundaries arise as natural conditions in the variational formulation,[7] i.e. $\partial\psi/\partial n = 0$, which is consistent with the requirement of normal flow there.

From symmetry considerations, the inlet and outlet boundaries may conveniently be made to coincide with a trough and crest or vice versa. This results in a reduced computational domain of length $\lambda/2 = L$.

As in Reference 13 we choose, here, the wave amplitude A as the representative quantity characterizing a computed wave for prescribed values of the parameters Q and λ. A is defined, as usual, as half the wave height. An alternative amplitude A_0 may be defined as the height of the wave crest h_{crest} above that of the asymptotic level D_0. A and A_0 are not identical, but they both represent adequately the wave profile, at least for waves of finite λ.

Most computed results will be presented through curves $(\lambda, A)_Q$ where Q and λ are prescribed and A emerges as a result of computation. Each point on the curve represents a wave of amplitude A, wavelength λ and discharge Q, which is held constant.

Each curve $(\lambda, A)_Q$ emanates from the asymptotic level D_0 at $\lambda = \lambda_0$ and rises until the highest possible wave of discharge Q is reached. The problem may thus be interpreted as a two-parameter bifurcation problem,[13] where D_0 is the trivial solution from which the bifurcation branch $(\lambda, A)_Q$ emanates at the bifurcation point $\lambda = \lambda_0$.

Coarse or distorted meshes have a significant effect on the computation of the curves $(\lambda, A)_Q$ (sets of waves of constant discharge Q). Even in the vicinity of $\lambda = \lambda_0$, where the solution can be obtained from linear theory, the inaccuracy resulting from the use of inadequate meshes could be large, as reported in Reference 15.

The main theme of this paper is to report on the effect that meshes have on the computation of branches $(\lambda, A)_Q$, for values of Q, as the amplitude becomes larger.

We do not consider the problem of computing explicitly the turning points. This is a problem that requires special treatment[16] and is outside the scope of the present work.

Concerning the fundamental aspects of bifurcation theory the interested reader should consult other sources.[17]

3. COMPUTATIONAL DETAILS AND MESH CONSIDERATIONS

The wave computations of this paper were carried out using a new Kantorovich method, the details of which are reported elsewhere.[12] In essence, the method consists of taking N terms of a Kantorovich expansion for the functional J given by equation (1). By using the stationary conditions for J one obtains a set of N non-linear ordinary differential equations in x for the position of N streamlines including that of the free surface.

The method could also be viewed as a semidiscretization of the flow domain in the y direction into N streamlayers bounded by N streamlines whose position is to be computed.

The resulting boundary value problem is then discretized in x by approximating derivatives by central differences at M equally spaced stations along x.

The set of $N \times M$ non-linear algebraic equations is solved by a Newton–Raphson iteration procedure. The algorithm was implemented in double precision on the AMDAHL 470 Computer of the University of Leeds. The algorithm is stable and convergence is fast.

An illustrative example is shown in Figure 1 for $Q^2 = 0{\cdot}2521952$ and $\lambda = 2{\cdot}3935979$ using $N = 48$ streamlines (48 terms in the Kantorovich expansion) and $M = 80$ stations. The computed amplitude is $A = 0{\cdot}1629698$. As indicated previously, computations are performed for half a wavelength and $b(x) = -1$ in equation (2) (horizontal bed).

The choice of the number of terms N in the expansion (or the number of streamlines) and the number of stations M completely determines a discretization of the two-dimensional flow

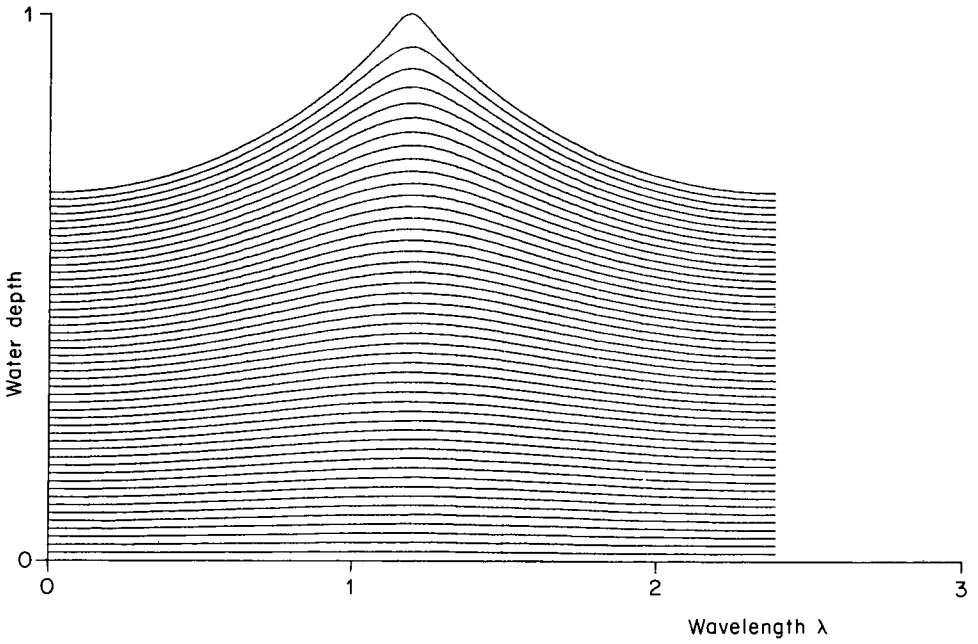

Figure 1. Computed large amplitude wave for $Q^2 = 0{\cdot}2521952$ and $\lambda = 2{\cdot}3935979$ using a 48×80 mesh

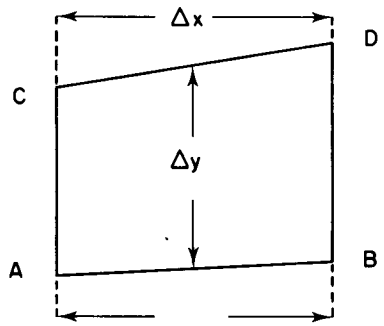

Figure 2. Typical element in final discretization of a two-dimensional flow domain

domain. Hence we speak of an $N \times M$ mesh and this is the meaning of mesh that is adopted in this paper.

Elements are quadrilateral regions as depicted in Figure 2. For a given $N \times M$ mesh the length $\Delta x = L/(M-1)$ is constant, but Δy varies from element to element and within an element as shown in Figure 2.

The horizontal length Δy also varies from iteration to iteration when solving the non-linear problem to find the positions of the N unknown streamlines. Segments AB and CD in Figure 2 are approximations to streamlines and thus the variation of Δy in the iteration procedure.

For the case of a limiting small amplitude wave the N streamlines are (almost) uniformly distributed in the y direction and therefore $\Delta y \simeq D_0/N$ where D_0 is the asymptotic level.[13] As the amplitude A increases Δy increases for elements near the vertical transversal through the wave crest and decreases for elements near the transversal through the wave trough. Nevertheless, the constant $(\Delta y)_0 = D_0/N$ is an adequate indication of the possible Δy values to be expected in both small and large amplitude waves.

In this paper we consider two types of mesh variations, namely mesh refinement and aspect ratio variation. We shall not consider mesh gradation other than that resulting from the self-adjusting character of the algorithm being employed.

The adequacy of a given $N \times M$ mesh will depend on the wave region being considered. Theoretical observations[15] indicate that short waves, for instance, exhibit an exponential variation of horizontal velocity with depth. Adequate simulation of such waves will therefore require a fine resolution in the y direction. The implication is that the number of streamlines N should be large in some sense. It is also known that long waves will be less demanding on the number N, for the variation of the horizontal velocity component $u = u(x, y)$ with y is less pronounced than for shorter waves. In fact the assumption $u = u(x)$ is a good approximation in the long wave region.[18,19]

For our numerical experiments we have chosen examples that are typical of the various wave regions.

4. MESH VARIATIONS

Here we report on the effect that mesh variations (aspect ratio variation and mesh refinements) have on the computed waves. The effects to be assessed are those on the wave amplitude A, i.e. on the curves $(\lambda, A)_Q$. Comparison of computed results with those of other investigators[3,14] will be carried out for some of the examples reported on in this paper. Also, an indirect assessment of errors will be performed by checking the dynamic boundary condition on the free surface, as done by Betts and Assaat.[11]

4.1. Effect on curves $(\lambda, A)_Q$

As indicated in section 2 the curves $(\lambda, A)_Q$, which are an indication of the computed wave profiles and thus wave amplitudes, may be, to a large extent, dependent on the particular $N \times M$ mesh being used. This mesh dependency will be illustrated here for various examples.

Example 1. $Q^2 = 0{\cdot}1400463$. The corresponding value of the asymptotic level is $D_0 = 0{\cdot}9166667$ and the bifurcation point is at $\lambda_0 = 1{\cdot}04723$.[13]

This example was first computed by Southwell and Vaisey[1] in 1946 using relaxation methods. In their algorithm they prescribed A and computed λ. We do the opposite. They computed ten points (waves) on the curve $(\lambda, A)_Q$ starting from the highest wave. Their results gave an overestimated solution for the infinitesimal amplitude wave (the bifurcation point). In a previous paper[15] we analysed in some detail the behaviour of the curves $(\lambda, A)_Q$ near the limiting small-amplitude wave, for various meshes. Here we shall pay attention to the larger-amplitude wave part of the same curves.

In Figure 3 we illustrate the computed curves $(\lambda, A)_Q$ for three different meshes: 18×10, 36×20 and 72×40. The computed points of Southwell and Vaisey are also shown there. Several comments on the results of Figure 3 are in order. First we note that the curves $(\lambda, A)_Q$ do not vary significantly with the mesh refinements. In fact the two finest meshes (36×20 and 72×40) give curves that are almost indistinguishable for most of the λ-range considered. Differences are more noticeable near the highest wave and near the infinitesimal amplitude wave ($\lambda = \lambda_0$), whose position in the Figure was computed from the linear theory.

The curve computed with the finest mesh (72×40) exhibits an inflexion point near the stagnation level. This feature, which was not detected by the coarser meshes, appears to be common to curves $(\lambda, A)_Q$ in the deep water region B_1, where bifurcation is to the left.[13]

The results of Southwell and Vaisey[1] for this example, also plotted in Figure 3, differ considerably from our three solution curves. Curiously, the differences are larger for the smaller-amplitude waves than for the larger-amplitude waves. Their infinitesimal-amplitude wave, obtained by extrapolation, is 6 per cent higher than the exact solution given by the Stokesian linear theory. Their solution for the highest wave, however, is probably very accurate. This can be seen from our results and those of Cokelet.[3] In section 4.3 we give more details about

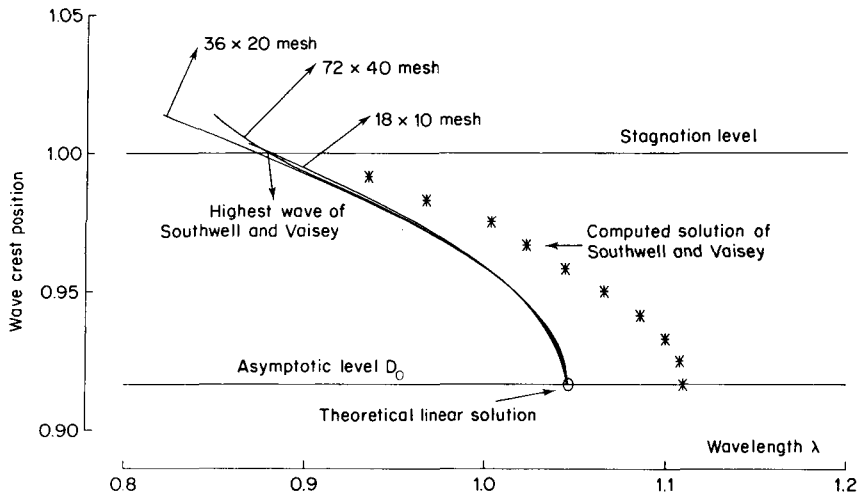

Figure 3. Computed curves $(\lambda, A)_Q$ for $Q^2 = 0{\cdot}1400463$ using three meshes

comparison of results for this and other highest waves and the way we compute them. It is nevertheless illustrative to indicate here the computed values for the wavelength λ_m of the highest wave (crest at stagnation level). The solution of Reference 1, quoted to 2 decimal places, is $\lambda_m = 0{\cdot}88$; our solution is $\lambda_m = 0{\cdot}8810526$ using the 72×40 mesh.

Example 2. $Q^2 = 0{\cdot}2691909$. In this case the asymptotic level is $D_0 = 0{\cdot}7771403$ and $\lambda_0 = 3{\cdot}0339155$. This example lies in an intermediate wave region B_2 where the curves $(\lambda, A)_Q$ bifurcate to the right and have a right turning point at amplitudes less than those of the corresponding highest waves. In Figure 4 we show a set of computed wave profiles for various wavelength values starting from $\lambda = \lambda_0$, which gives the zero-amplitude wave. As λ is increased the amplitude A increases. There is a range of λ values that give double solutions within the range of physical interest, i.e. for a given value of λ in this range there are two solutions of the same wavelength, and the same discharge Q, but of different amplitudes.

The effect of mesh refinements on the computed curve $(\lambda, A)_Q$ is significant in this example. As for example 1, we consider here three different meshes, namely 10×30, 20×60 and 40×120. The corresponding computed curves are illustrated in Figure 5. The actual computed points (waves) are also shown there.

The curves are almost indistinguishable for waves ranging from the zero-amplitude wave to those of moderately large amplitude. As the amplitude continues to increase the difference becomes dramatic. Note for instance that the estimated position of the turning point is about 4 when using the 40×120 mesh, about 5 when using the coarser mesh (20×60) and about 9 for the coarsest mesh (10×30). In preliminary computations for this example using the 10×30 mesh we considered the possibility of finding the highest wave by extrapolation, since at that time we did not know the behaviour of the curve near the stagnation level. The results of Figure 5

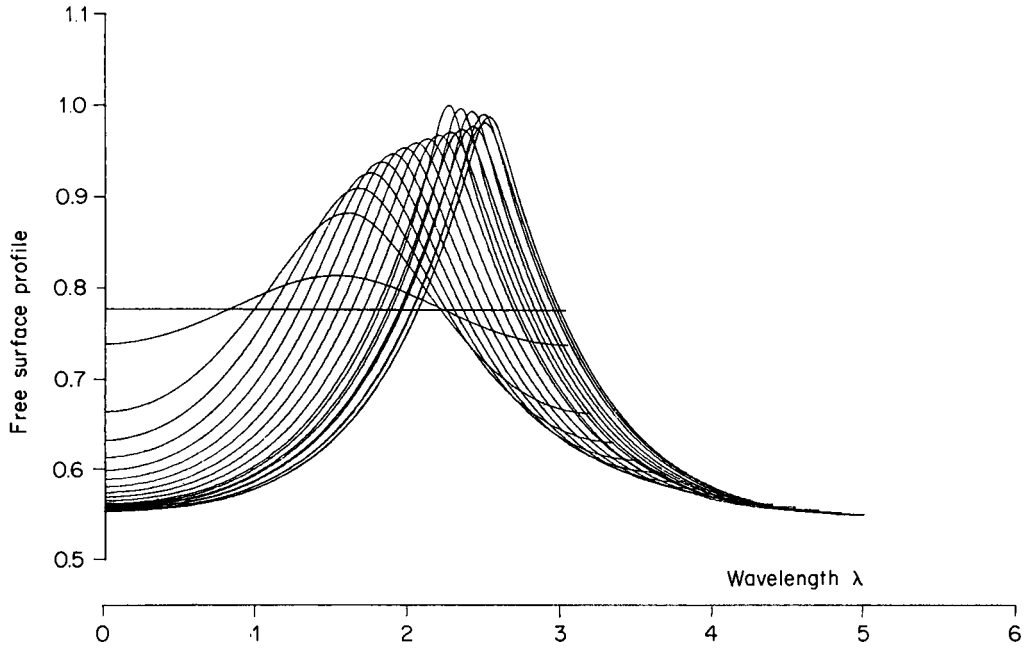

Figure 4. Computed free surface profiles for $Q^2 = 0{\cdot}2691909$ and various values of λ using a 20×60 mesh. Double values of solutions occur

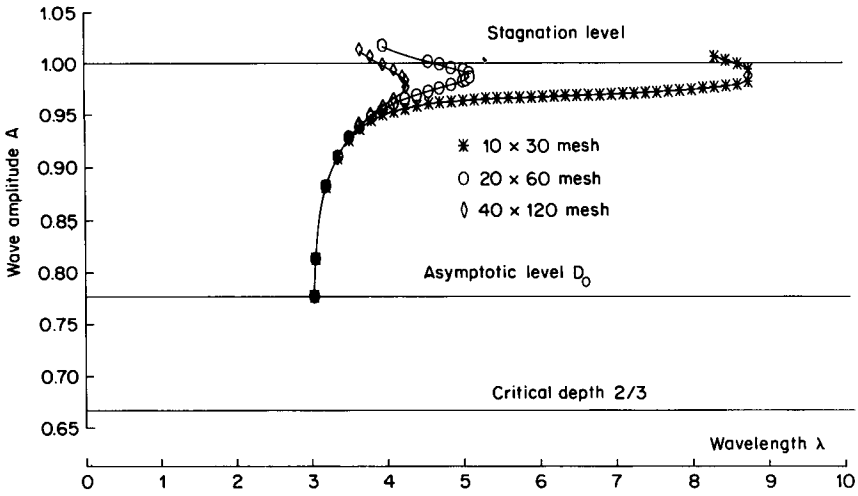

Figure 5. Computed curves $(\lambda, A)_Q$ for $Q^2 = 0{\cdot}2691909$ using three meshes

give a clear warning about the use of extrapolation procedures to calculate large-amplitude wave properties, at least in B_2.

Computations for this example are very accurate for the small-amplitude waves for all the three meshes considered as compared with the linear theory. For waves with crests near the stagnation level, only fine meshes will give accurate results. Comparisons will be made later in section 4.3.

Example 3. $Q^2 = 0{\cdot}296295$. The corresponding asymptotic level for this example is $D_0 = 0{\cdot}6674865$ and $\lambda_0 = 39{\cdot}6492024$. Branching is to the right, i.e. the amplitude A increases monotonically with the wavelength λ.

For this shallow-water example the effect of meshes on the computed curve $(\lambda, A)_Q$ is not significant. In Table I computed results for three mesh configurations are shown. The wave-amplitude A there is $A = (h_{\text{crest}} - h_{\text{trough}})/2$. Variations of the alternative amplitude $A_0 = h_{\text{crest}} - D_0$ with mesh refinements are found to be practically negligible.

From Table I one can see that the effect of refining the mesh is to reduce the wave amplitude very slightly. The effect is shown in the 7th decimal place and only for the higher waves, at the first refinement level. The finest mesh (12 × 360) leaves the results of the 6 × 180 mesh unaltered, except for the case $\lambda = 47{\cdot}6$.

For this example we also performed computations using $N = 1$, i.e. a single layer. This would correspond to a shallow-water model, as discussed in Reference 19. It can be anticipated that results should not differ significantly from those in Table I obtained from multilayer meshes ($N > 1$). In Table II we show computed results using four one-layer meshes.

Computed values from the single-layer meshes of Table II do not differ considerably from those of Table I. The difference appears in the 6th decimal place. For instance, the case $\lambda = 46{\cdot}7$ has solutions for the wave height $2A$ with errors of $\pm 0{\cdot}07$ per cent relative to the finest mesh solution of Table I. More about this will be said later when we compare results against the Cnoidal wave theory[14] and discuss the aspect ratio influence.

4.2. Assessment of errors

In this section we carry out an indirect assessment of errors and discuss the suitability of meshes for the different wave regions. First we shall assess errors by checking the dynamic

Table 1. Computed values $2A \times 10^3$ for $Q^2 = 0{\cdot}296295$ using three meshes. Amplitude is $A = (h_{\text{crest}} - h_{\text{trough}})/2$

λ	Mesh 3 × 90	6 × 180	12 × 360
40·4	0·6124	0·6124	0·6124
41·2	0·9135	0·9134	0·9134
42·0	1·1185	1·1184	1·1184
42·8	1·2764	1·2763	1·2763
43·6	1·4048	1·4047	1·4047
44·4	1·5122	1·5122	1·5122
45·2	1·6041	1·6040	1·6040
46·0	1·6836	1·6835	1·6835
47·6	1·8147	1·8147	1·8147
48·0	1·8428	1·8427	1·8427

Table II. Computed values $2A \times 10^3$ for $Q^2 = 0{\cdot}296295$ using four one-layer meshes

λ	Mesh 1 × 30	1 × 90	1 × 180	1 × 360
40·4	0·6150	0·6061	0·6053	0·6051
42·0	1·1200	1·1155	1·1155	1·1150
43·6	1·4060	1·4027	1·4024	1·4024
45·2	1·6052	1·6025	1·6023	1·6022
46·8	1·7544	1·7520	1·7518	1·7517
47·6	1·8158	1·8136	1·8134	1·8133
48·4	1·8704	1·8683	1·8681	1·8681
55·6	2·1743	2·1726	2·1724	2·1724

boundary condition on the free surface as done by Betts and Assaat.[11] This procedure, although indirect, provides an idea of the self-consistency of the computed results. The other way we shall assess errors here will be by comparing some of our computed results with those of other investigators. To this end we shall consider three examples of highest waves and compare our computed results with those of Cokelet.[3] Also we shall compare some other examples with the cnoidal wave theory of Benjamin and Lighthill.[14]

Dynamic boundary condition. The stationary conditions of the functional J given by equation (1) give a second boundary condition (the dynamic boundary condition) on the free surface $y = -1 + h(x)$. In our units and frame of reference this takes the form

$$\tfrac{1}{2}U_s^2 + y = 0, \tag{3}$$

where U_s denotes the surface velocity.

An estimate of errors is given by evaluating the left hand side of equation (3). This corresponds to a total head error and will be denoted by ΔH.

In the approximation of the present paper the velocity $U = (u, v)$ within an element, such as that illustrated in Figure 2, is given by[12]

$$u = -\frac{\partial \psi}{\partial y} = -Q/Nh_i, \tag{4}$$

$$v = -\frac{\partial \psi}{\partial x} = Q(h_i y'_{i-1} - h'_i(y_{i-1} - y))/(Nh_i^2).$$

h_i denotes the element width Δy, y_{i-1} denotes the position of the base of the element and denotes differentiation with respect to x. For a surface element equations (4) reduce to

$$\begin{aligned} u &= -Q/(Nh_N), \\ v &= Qy'_N/(Nh_N). \end{aligned} \tag{5}$$

In assessing the total head error ΔH we have taken U_s, the velocity at the free surface, as that within a surface element and given by equations (5). Such value for U_s will result in an exaggerated error ΔH. This can be seen, for instance, by considering U_s at the wave crest where $v = 0$. U_s depends only on the horizontal velocity component u which decreases with depth. Thus the value for U_s from equations (5) is somewhat larger than the exact value at the surface. Similarly, at the wave trough U_s, as given by (5), is somewhat smaller than the exact value, since u increases with depth.

For example 1 of section 4.1 ($Q^2 = 0{\cdot}1400463$) we computed the estimated total head error ΔH at various stations along the wave surface using three different meshes (9×6, 18×11 and 36×21).

In Figure 6 we illustrate the variation of ΔH along the free surface for a wave of wavelength $\lambda = 0{\cdot}93$. The error ΔH is observed to decrease as the mesh is refined. By halving the mesh size, in both directions, $(\Delta H)_{max}$ is approximately halved. This is illustrated by observing values at the crest and trough in Figure 6.

Clearly errors are largest at the wave trough and at the wave crest. From the comments following equations (5) it is reasonable to suppose that the resulting error wave (Figure 6) has an amplified amplitude resulting from the estimated surface velocities.

Numerical results also show that the maximum total head error $(\Delta H)_{max}$ increases as the wave amplitude increases, i.e. errors are largest for the highest waves. In Figure 7 we plot ΔH at the trough (negative) and at the crest (positive) against the wave height $2A$ for three meshes. Again, by performing mesh refinements $|\Delta H|$ is decreased, as one would expect.

The estimated total head errors ΔH at the free surface for the example considered are similar to those of Betts and Assaat.[11] This is not surprising since their finite element algorithm is of similar accuracy to our discretized Kantorovich method. Their tabulated results (their Table 6.1) refer to different wave examples lying more towards the shallow-water wave region and thus no direct comparison of results can be made here. Nevertheless, their first example

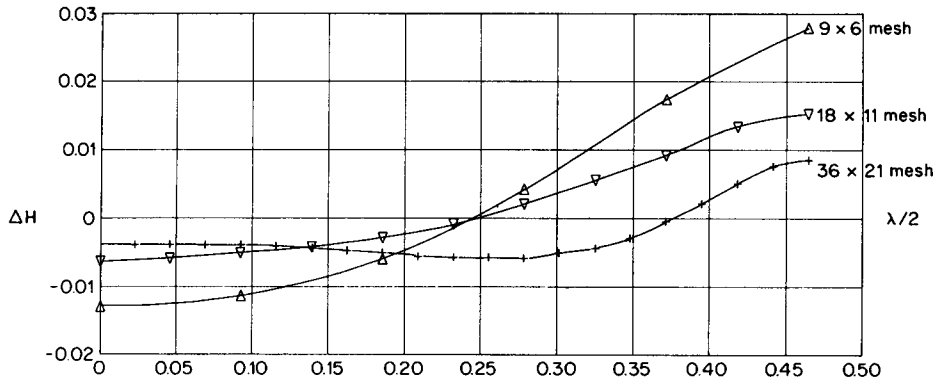

Figure 6. Estimated total head error ΔH for $Q^2 = 0{\cdot}1400463$, $\lambda = 0{\cdot}93$ using three meshes

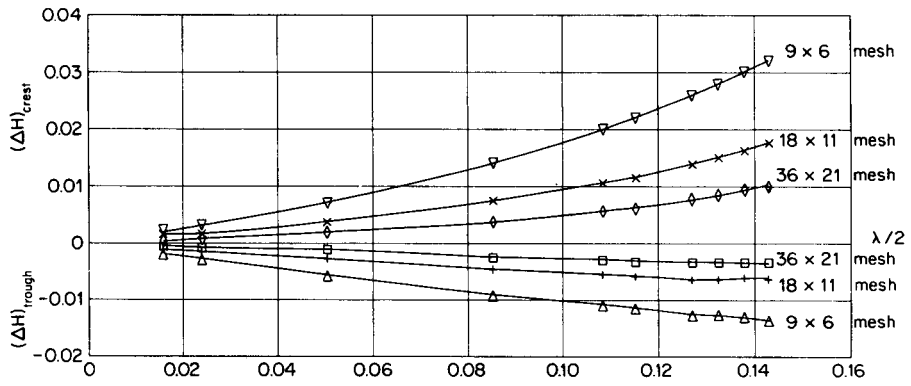

Figure 7. Plot of $(\Delta H)_{trough}$ and $(\Delta H)_{crest}$ against wave height $2A$ for $Q^2 = 0{\cdot}1400463$ using three meshes

$(\exp(-d_s) = 0{\cdot}2)$ being the closest to ours, could be taken for an indirect comparison. Their 10×6 mesh (in our notation) gives $(\Delta H)_{max} = 0{\cdot}038$; our 9×6 mesh gives $(\Delta H)_{max} = 0{\cdot}032$ for a wave close to the highest (see Figure 7). Reductions in $(\Delta H)_{max}$ by mesh refinements are observed to be similar to ours. It should be pointed out however, that the meaning of a mesh $N \times M$ for the examples being compared are not equivalent in the sense that deep and shallow water waves have different mesh requirements (e.g. aspect ratio) for a desired accuracy.

Highest waves. Here we assess discretization errors and effects of mesh refinements for three highest-wave examples. A comparison with the computed results of Cokelet[3] is carried out in an indirect fashion. A reliable curve-fitting technique involving cubic splines is applied to Cokelet's ten-point data for waves of greatest height. Direct evaluation at the desired values of the independent variable will give appropriate values for comparison.

The quantities subject to comparison are the ratio wavelength to depth λ/D and the ratio wave height to wavelength $2A/\lambda$ (wave steepness). We take the relative wavelength λ/D as the independent variable and the wave steepness as the dependent quantity subject to comparison. In Table III we show our computed results for the wave steepness for given relative wavelengths and the corresponding interpolated values from Cokelet's data. The chosen wave examples have relative wavelength less than about six and lie in the wave region where the 110-term series of Cokelet is most accurate.

In Table III it can be seen that the relative error is reduced by half when the mesh size in both directions is halved, a result that was also observed for the estimated total head error in

Table III. Comparison of results of wave steepness $2A/\lambda$ for waves of greatest height

Q^2	$N \times M$	λ/D	$2A/\lambda$ this paper	$2A/\lambda$ Cokelet
0·1400463	18 × 10	0·9785806	0·1523002	0·1431783
	36 × 20	0·9690463	0·1485016	0·1431765
	72 × 40	0·9741159	0·1448542	0·1431775
0·2521952	24 × 40	3·1887330	0·1381528	0·1346546
	48 × 80	3·1744905	0·1362655	0·1347619
0·2691909	20 × 60	7·1969956	0·0955807	0·0942090
	40 × 120	5·8624666	0·1080545	0·1074530

section 4.2. In the first example with $Q^2 = 0{\cdot}1400463$ the relative error is 6·4 per cent for the coarsest mesh (18 × 10) and 1·17 per cent for the finest mesh (72 × 40). Similar variations are observed in the other examples. Our results are consistently higher than those of Cokelet, with agreement tending to improve as the relative wavelength increases. The second example, $Q^2 = 0{\cdot}2521952$ gives a relative error of 1·1 per cent for the finest mesh, whereas the third example gives an error of 0·6 per cent when using the finest mesh (40 × 120).

Results show that the algorithm being used here is capable of giving results of comparable accuracy to the highly accurate results of Cokelet. Fine meshes must be used, however.

It would appear as if our algorithm were more adequate for wave ranging from the intermediate wave region to the long wave region than for waves in the deep water region. Waves in the latter region require fine meshes, in particular more layers (larger N), in order to model the exponential variation of velocities; and larger N values increase the bandwidth of the Jacobian matrix. Thus it is more expensive, in storage and CPU time, to compute accurately deep-water waves than it is to compute other waves.

Cnoidal waves. Here we compare some of our computed results with the cnoidal wave theory of Benjamin and Lighthill.[14] In this theory the wave profile is given in terms of a non-linear ordinary differential equation involving three parameters, namely the total head, the discharge and the momentum.

In order to compare results directly we solved their non-dimensionalized equation (23) numerically, using central differences and treating the resulting non-linear algebraic equations in a similar fashion to that of the present algorithm.[12]

In Table IV we show our computed results and those obtained from Benjamin and Lighthill's equation for $Q^2 = 0{\cdot}2945430$.

Our results in Table IV were obtained using an 18 × 100 mesh, i.e. 18 layers and 100 stations. The cnoidal wave equation of Reference 14 was also solved using 100 stations. Our amplitudes are slightly larger than those of Benjamin and Lighthill, less than 1 per cent of relative error. It is interesting to note, however, that results compare very well for the position of the wave crest. For instance, for $\lambda = 12{\cdot}0$ our result is $y_{\text{crest}} = 0{\cdot}7274687$ and that of Reference 14 is $y_{\text{crest}} = 0{\cdot}7267286$ with a relative error of 0·1 per cent. For $\lambda = 8{\cdot}0$ the wave crest relative error is only 0·08 per cent. Our profiles have slightly deeper troughs than those of Benjamin and Lighthill.

It is not certain whether the results evaluated from the theory of Reference 14 and given in Table IV are less accurate than our own, since we may have introduced an error in these results when supplying the parameter S (the horizontal momentum corrected for pressure forces and divided by the density) calculated from our computed results. In principle, however, our algorithm should be more accurate, for it represents are full (ideal) non-linear theory. By observing the mesh refinement effects for example 3 of section 4.1 one can see that for a fixed number of

Table IV. Comparison of results with cnoidal wave theory

λ	λ/D	Amplitude A this paper	Amplitude A Reference 14	Percentage error
8·0	11·71661	0·0349368	0·0346478	0·8
9·0	13·29546	0·0397768	0·0394348	0·86
10·0	14·87026	0·0421978	0·0418339	0·86
11·0	16·44300	0·0435263	0·0431512	0·86
12·0	18·01475	0·0442930	0·0439094	0·87

stations M, increasing the number of layers N has the effect of increasing the amplitude A. This appears to be a general feature in the shallow water region. Thus one can think of our 18×100 mesh for the present example as representing the correct trend. The third order theory of Reference 14 could be closely represented by taking $N = 3$ (three terms in the Kantorovich expansion) in our model. This would have the effect of decreasing our computed amplitude values.

5. DISCUSSION

In this paper we have given special consideration to the problems of (i) computing the bifurcation curves $(\lambda, A)_Q$ and (ii) analysing the effects that mesh variations may have on the computation of the curves. Other wave properties, such as steepness, velocity, etc., may not have identical mesh requirements as the bifurcation curves $(\lambda, A)_Q$.

Three wave regions B_1, B_2 and B_3 can be identified, each one having its own mesh requirements. Results presented here indicate that curves $(\lambda, A)_Q$ in B_1 are not significantly affected by mesh refinements (Figure 3). All three meshes considered in example 1 (section 4.1) in the region B_1 give curves that are almost indistinguishable from each other throughout the entire range of wave amplitudes. A careful examination of results, however, indicates that the finest mesh used detects an inflexion point at a distance short of the highest wave. The existence of such an inflexion point appears to be a common feature to all curves $(\lambda, A)_Q$ in B_1 as illustrated by other computed results reported on in Reference 13.

Adequate representation of other wave properties in B_1 (e.g. steepness, velocity) necessitates fine meshes. For instance, the well-known[3] existence of a maximum for the velocity at nearly breaking point is confirmed in the present study, but only when using the finest mesh, in example 1.

The indirect assessment of total head errors carried out in section 4.2 gives another indication of the level of mesh refinements that are necessary for computing reliable results. Wave crests and troughs are seen to require better resolution than other wave zones and special mesh refinement/gradation would appear to be needed. We have not done this since the algorithm used in the present work assumes a semi-uniform mesh throughout the computational domain. Departure from uniformity results from the self-adjusting feature of the streamlines in the model. The work of Betts and Assaat[11] shows, however, that mesh gradation, as a substitute for straight mesh refinement, does not greatly increase accuracy.

The comparison of results with those of Cokelet[3] for waves of greatest height (section 4.2) gives a more precise idea of the relationship between mesh size and accuracy.

The aspect ratio $R = (M-1)/N$ (where M is the number of stations and N the number of streamlines) is, in addition to the mesh sizes Δx and Δy, an important parameter in the discretization of the flow domain. As with Δx and Δy the region B_1, B_2 and B_3 have different requirements on the mesh parameter R.

Meshes for computing curves $(\lambda, A)_Q$ in B_1 should provide a good resolution in the y-direction, which roughly means that more importance should be given to the number of streamlines N than to the number of stations in the model. This is partially explained by the way in which the horizontal component of velocity u varies with depth in the region B_1 of deep-water waves. For example 1, $R = \frac{1}{2}$ for all meshes and $0{\cdot}049 < \Delta x < 0{\cdot}058$ for the coarsest mesh used and $(\Delta y)_0 \simeq 0{\cdot}051$; $\Delta x/(\Delta y)_0 \simeq 1$. Notice that Δx depends on the wavelength, for a fixed $N \times M$ mesh. Numerical experiments for the lower part of the curve $(\lambda, A)_Q$, reported elsewhere,[15] show that for values of R greater than about $\frac{2}{3}$ results in loss of accuracy and the solution curve could give an infinitesimal wave that is far too long when compared with the exact theory at $\lambda = \lambda_0$.

We now turn to curves $(\lambda, A)_Q$ that belong to the intermediate wave region B_2; they have

turning points and, in contrast to curves in B_1, are very sensitive to mesh refinements. Example 2 (section 4.1) in this region illustrates the difference very clearly (Figure 5). It is pointed out, however, that mesh refinement effects are practically negligible for the smaller amplitude waves, i.e. the lower part of the curves. For the upper part of the curves the effect is striking. Consider for instance the location of the critical value of the parameter λ where the turnning point occurs.

Other wave properties also require fine meshes in order to be accurately represented. This is well illustrated by the comparison of results for highest waves in Table III. The finest mesh used there gives a wave steepness that is 1 per cent higher than Cokelets's solution.

The aspect ratio R for example 2 in the region B_2 is about 3 (for all meshes used); for the coarsest mesh (12×20) $(\Delta y)_0 \simeq 0{\cdot}065$ and $0{\cdot}16 < \Delta x < 0{\cdot}4$, i.e. $\Delta y/\Delta x$ is significantly less than one.

Curves $(\lambda, A)_Q$ in the wave region B_3, where bifurcation is to the right, are not greatly affected by mesh refinements. The computed results for example 3 illustrate this well; for these, as observed in Table I, the mesh refinement effects are practically negligible. The aspect ratio for this example is 30 and, for the coarsest mesh, $(\Delta y)_0 \simeq 0{\cdot}222$ and $0{\cdot}45 < \Delta x < 0{\cdot}54$. Fine resolution in the y-direction appears not to be required when computing curves in B_3, in contrast to curves in B_1. Again this may be partially explained by the way in which the horizontal component of velocity u varies with depth in the shallow water region.

Table II illustrates the fact that in the extreme case of a model with one layer $(N = 1)$ we still obtain solution curves that are reasonably accurate when compared with solutions obtained from models including more layers $(N > 1)$. In fact, as discussed in Reference 19, the case $N = 1$ constitutes a shallow-water (non-linear) approximation.

Changes in the values of the aspect ratio R produce changes in the results, as one would expect, but such an effect for example 3 is not dramatic. The results for $R = 30$, 90, 180 and 360 are illustrated in Table II. A careful comparison of the results of Tables I and II suggests that the most accurate solution curve 12×30 mesh would lie somewhere between those obtained with the 1×30 and 1×90 meshes. It would appear, therefore, that by increasing R to values 180 and 360 one would spoil the solution.

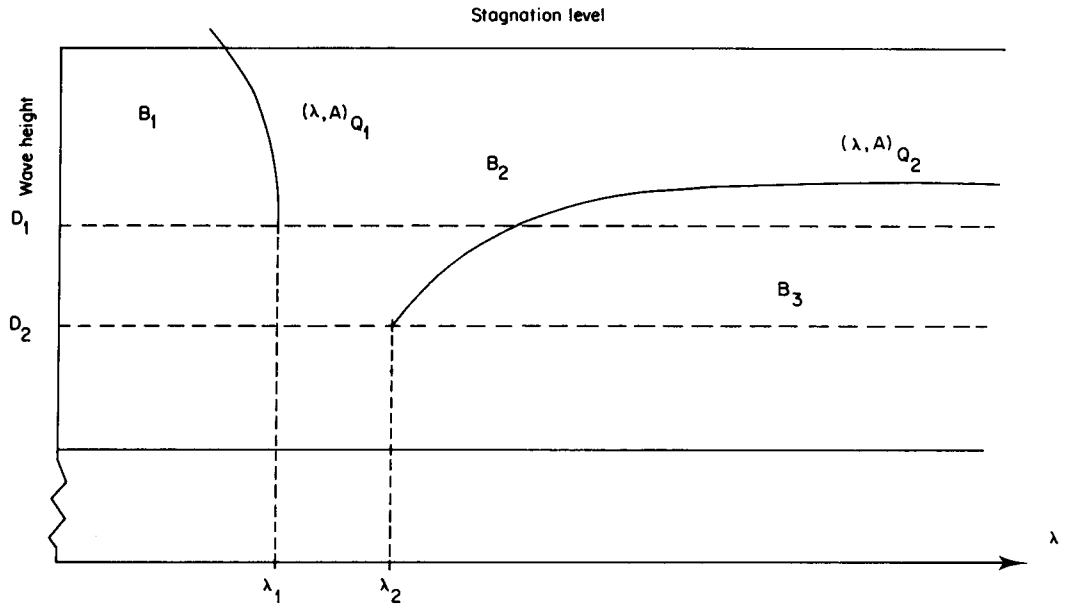

Figure 8. Sketch of transition bifurcation branches defining B_1, B_2 and B_3

5. CONCLUSIONS

The computational technique used in this paper is capable of producing accurate results for waves of all amplitudes and all finite wavelengths.

The effect of mesh refinements on the solution curves $(\lambda, A)_Q$ is dependent upon the wave region under consideration. Three regions B_1, B_2 and B_3 are identified. Curves in B_1 are not particularly sensitive to mesh refinements; the same is true for curves in B_3. Curves in the intermediate wave region B_2, however, are very sensitive to mesh refinements; this is specially the case for the larger-amplitude waves, in the vicinity of turning points.

The aspect ratio R is found to be an important mesh parameter. Results indicate that adequate values of R should increase monotonically as one moves from B_1 towards B_3.

Other wave properties, such as wave steepness and velocity, always require fine meshes. For the smaller-amplitude waves, however, regardless of the wave region, coarse meshes can provide reasonable solutions for these wave properties as well as for the curves $(\lambda, A)_Q$.

ACKNOWLEDGEMENTS

This work was carried out while the author was employed at the University of Leeds, Department of Applied Mathematical Studies. The financial and academic support provided are gratefully acknowledged.

The author also thanks Dr M. J. O'Carroll, Mathematics Department, Teesside Polytechnic, for his useful comments during discussions on the present and related problems.

REFERENCES

1. R. V. Southwell and G. Vaisey, 'Relaxation methods applied to engineering problems XII. Fluid motions characterized by free streamlines', *Phi. Trans. Roy. Soc.*, **A240,** 117–161 (1946).
2. L. W. Schwartz, 'Computer extension and analytic continuation of Stokes' expansion for gravity waves', *J. Fluid. Mech.*, **62,** pt. 3, 553–578 (1974).
3. E. D. Cokelet, 'Steep gravity waves in water of finite depth', *Phil. Trans. Roy. Soc.*, **A286,** 183–230 (1977).
4. M. S. Longuet-Higgins, 'Integral properties of periodic gravity waves of finite amplitude', *Proc. Roy. Soc. London*, **A342,** 157–174 (1975).
5. J. G. B. Byatt-Smith and M. S. Longuet-Higgins, 'On the speed and profile of steep solitary waves', *Proc. Roy. Soc. London*, **A350,** 175 (1976).
6. J. M. Williams, 'Limiting gravity waves in water of finite depth', *Phil. Trans. Roy. Soc. London*, **A302,** 139–188 (1981).
7. M. J. O'Carroll and H. T. Harrison, 'Variational techniques for free streamline problems', *Proc. 2nd International Symposium on Finite Elements in Flow Problems*, Genoa, Italy, 1976, pp. 485–495.
8. M. Ikegawa and K. Washizu, 'Finite element analysis of flow over a spillway crest', *Int. j. numer. methods eng.*, **6,** 179–189 (1973).
9. J. M. Aitchison, 'A finite element solution for critical flow over a weir', *Proc. 3rd International Conference on Finite Elements in Flow Problems*, Banff, Alberta, Canada, 1980.
10. E. F. Toro, 'Finite element computation of free surface problems', *Ph.D. Thesis*, Department of Mathematics and Statistics, Teesside Polytechnique, U.K., 1982.
11. P. L. Betts and M. I. Assaat, 'Large-amplitude water waves', in R. H. Gallagher *et. al.* (eds) *Finite Elements in Fluids, Vol. 4*, Wiley 1982, pp. 109–127.
12. E. F. Toro and M. J. O'Carroll, 'A Kantorovich computational method for free surface gravity flows', *Int. j. numer. methods fluids*, **4,** 1137–1148 (1984).
13. E. F. Toro, 'Transition bifurcation branches in non-linear water waves', *Int. j. numer. methods in fluids*, **6,** 219–228 (1986).
14. T. B. Banjamin and M. J. Lighthill, 'On cnoidal waves and bores', *Proc. Roy. Soc. London*, **A224,** 448–460 (1955).
15. E. F. Toro and M. J. O'Carroll, 'Mesh effects on the computation of small-amplitude water waves', *Int. j. numer. methods fluids*, **5,** 505–513 (1985).
16. A. Griewank and G. W. Reddien, 'Characterization and computation of generalised turning points', *SIAM J. Numer. Anal.*, **21,** (1), 176–185 (1984).
17. I. Stakgold, 'Branching of solutions of non-linear equations', *SIAM Review*, **13,** (3), 289–332 (1971).
18. J. J. Stoker, *Water Waves*, Interscience Publishers Inc., New York, 1957.
19. M. J. O'Carroll and E. F. Toro, 'A simple variational approximation of shallow water type', *Applied Mathematical Modelling*, **8,** 261–264 (1984).